International Journal of Heat and Mass Transfer 66 (2013) 72–79

Contents lists available at SciVerse ScienceDirect

International Journal of Heat and Mass Transfer

journal homepage: www.elsevier.com/locate/ijhmt

Interactions between heat transfer, flow field and flame stabilization in a micro-combustor with a bluff body

Aiwu Fan [a,*], Jianlong Wan [a], Kaoru Maruta [b], Hong Yao [a], Wei Liu [a]

[a] State Key Laboratory of Coal Combustion, Huazhong University of Science and Technology, Wuhan 430074, China
[b] Institute of Fluid Science, Tohoku University, Sendai 980-8577, Japan

ARTICLE INFO

Article history:
Received 13 April 2013
Received in revised form 5 July 2013
Accepted 8 July 2013
Available online 31 July 2013

Keywords:
Micro-combustor
Bluff body
Blow-off limit
Heat conduction
Flow field
Flame stretching
Heat losses

ABSTRACT

We recently developed a micro bluff body combustor. Both experimental and numerical investigations demonstrated that the bluff body can significantly extend the blow-off limit. In the present paper, the effect of solid materials (i.e., quartz, stainless steel, and SiC) on the blow-off limit of this micro-combustor was investigated numerically. The results show that the blow-off limit of the quartz combustor is the largest, while that of the SiC combustor is the smallest. The underlying mechanisms were analyzed in terms of the interactions between the flow field, heat transfer processes and flame stabilization. It is demonstrated that when the thermal conductivity is small (i.e., quartz), less heat is conducted to the upstream walls, the fresh mixture is not sufficiently preheated and the gaseous volume does not expanded so significantly. Therefore, the flame stretching effect is weaker than the other two cases and thus a larger blow-off limit is achieved. Moreover, for the stainless steel and SiC micro-combustors, a larger thermal emissivity (i.e., SiC) results in a bigger 'total heat loss ratio' and a smaller blow-off limit. In summary, a solid material with relatively low thermal conductivity and emissivity is beneficial to obtain a large blow-off limit for the micro bluff body combustor. The present study also demonstrates that both flow and heat transfer processes, as well as their interactions, play an important role in flame stabilization of the micro bluff body combustor.

© 2013 Elsevier Ltd. All rights reserved.

1. Introduction

With the rapid development of micro-electro-mechanic system technology, many types of small devices, such as micro-aircrafts, robots, gas turbines, engines, and portable electronic devices have continuously appeared. As the electrochemical batteries have disadvantages of short life spans, long recharging periods and especially their low energy densities, combustion-based power sources are considered to be potential alternatives in the future due to the much higher energy densities of hydrocarbon fuels [1,2]. Therefore, combustions under micro- and meso-scales have attracted increasing attention during the last two decades [1,2].

However, there are several challenges to maintain stable flames in micro-combustors. The most important one is the increased heat losses due to large surface area-to-volume ratio [1–3]. By far, various kinds of unstable flames have been reported [4–15]. For instance, flames with repetitive extinction and ignition (FREI) of premixed CH_4/air mixture were observed in both straight channel and curved duct [4–6]. This combustion mode was later numerically reproduced [7–11]. In addition, some special flame patterns, such as rotating Pelton-wheel-like flames, spiral flame, and X-shaped spinning flames, were observed in micro- and meso-scale channels [12–17].

Up to now, tremendous efforts have been made to stabilize the flame in micro-combustors. Thermal managements, such as heat recirculation and heat losses control, are good approaches to overcome the negative effect of heat losses and sustain a stable flame in micro-combustors [18–25]. The "Swiss-roll" combustor which can utilize the thermal energy of burned hot gases to preheat the fresh mixture is an effective method in increasing flame speed and extending flammability limits of micro-combustors [18–20]. The thermal properties of the solid material play a significant role in flame stability of micro "Swiss-roll" combustors [18]. Stainless steel mesh was used by Li et al. [21] to anchor premixed H_2/air flame in a micro thermal photovoltaic system. Shi et al. [22,23] investigated combustion characteristics in the combustors with porous media. Jiang et al. [24] developed a miniature cylindrical combustor with porous wall. Flame can be stabilized in the combustor chamber due to the reduction of heat losses and preheating effect on the cold fresh mixture. Taywade et al. [25] utilized an external heating cup for heat recirculation in a three-step micro-combustor. It is shown that heat recirculation significantly enhances the flame stability.

* Corresponding author. Address: School of Energy and Power Engineering, Huazhong University of Science and Technology, 1037 Luoyu Road, Wuhan 430074, China. Tel.: +86 27 87542618; fax: +86 27 87540724.
E-mail addresses: faw@hust.edu.cn, faw_73@163.com (A. Fan).

0017-9310/$ - see front matter © 2013 Elsevier Ltd. All rights reserved.
http://dx.doi.org/10.1016/j.ijheatmasstransfer.2013.07.024

Utilizing the recirculation zone is another effective way to stabilize flame in micro-combustors. Yang et al. [26] and Pan et al. [27] developed micro-combustors with a backward facing step. The experimental results showed that the step is useful in controlling flame position and widening operational ranges. Khandelwal et al. [28] investigated premixed CH_4/air flame in micro-combustors with two backward steps. Their results showed that a stable flame can occur in wide ranges of inlet velocity and equivalent ratio. Wu et al. [29] proposed an improved design of a micro gas turbine engine which was originally developed by the MIT group [30]. They added an additional wafer of micro channel to regulate the velocity distribution and direction near the combustor entrance. Their numerical results indicate that the improved design can significantly extend the operating range of mass flow rate, which may lead to higher power density of the micro-combustor. Very recently, Fan and co-workers [31,32] developed a planar micro-combustor with a bluff body. The main concern of their work is the blow-off limit, which is an important index of the combustion limit, i.e., the largest inlet velocity before flame is blown out of the combustor. The experimental results show that the blow-off limit of H_2/air flame is extended by five times as compared with the straight channel. Numerical results of the blow-off limit also show reasonable agreement with the experimental data. This work demonstrates that the micro-combustor with a bluff body has a strong ability in flame stabilization. Veeraragavan and Cadou [33,34] showed that heat recirculation through combustor walls has a crucial effect on the temperature distribution and burning velocity in micro-combustors. The serial papers by Vlachos and co-workers [35–37] demonstrate that a high thermal conductivity of the walls leads to a large blow-off limit for the straight channel. Motivated by those works [33–37], we were dedicated to numerically investigate the effect of solid material on the blow-off limit of premixed H_2/air flame in the micro bluff body combustor. The underlying mechanisms were discussed from viewpoints of the interactions between the flow field near the bluff body, heat conduction in solid walls, heat losses from the outer walls, and flame stabilization.

2. Numerical method

2.1. Geometrical model

The cross section of the micro bluff body combustor is schematically shown in Fig. 1. The total length of the combustor (L_0) is 16.0 mm. The width (W_0) and height (W_1) of the combustor chamber are 10 mm and 1 mm, respectively. The thickness of combustor wall (W_3) is 1 mm. The cross section of the bluff body is an equilateral triangle with a side-length W_2. The bluff body is symmetrically located with respect to the upper and lower walls, and the distance from the vertical surface of the buff body to the combustor inlet (L_1) is 1 mm. The size of the bluff body is indicated by a dimensionless parameter, i.e., the blockage ratio $\zeta = W_2/W_1$. As the aspect ratio (W_0/W_1) of the combustor chamber is very large (10:1), we adopted a two dimensional model in our numerical simulation to reduce the computation load.

2.2. Mathematical model

As the characteristic length of the combustor chamber is still sufficiently larger than the molecular mean-free path of gases flowing through the micro-combustor, fluids can be reasonably considered as continuums and the Navier–Stokes equations are still suitable in the present study [38]. It is well known that the combustion is a very complicated process involving flow, heat transfer and chemical reactions. According to the classic book by Williams [39], the flame instability usually has two major types, i.e., thermo-diffusion instability and hydraulic instability. Many other factors, such as the interactions among heat, mass transfer and chemical reactions may also trigger a turbulent combustion. For the combustion under micro- and meso-scales, these interactions can be greatly enhanced due to the small space of the combustor chamber. Therefore, the flame isprone to be turbulent in micro-combustors and it is not suitable to judge a flame is a laminar one or a turbulent one just by the Reynolds number. We can list many experimental examples to support this. For instance, Kumar et al. and Fan et al. observed many kinds of unstable flame patterns, such as rotating Pelton-wheel-like flames, spiral flame, X-shaped spinning flame in micro- and meso-scale channels [12–15,23,26–28]. In these cases, the *Re* at the inlet port is controlled to be in the laminar regime, however, the flames are not laminar ones. Our recent experimental investigations on CH_4 combustion in the small bluff body combustor also demonstrated that the flame transited to a turbulent mode with flame pulsation and noise emission at a relatively low *Re* of 175. (Note: these data have not been published yet.) In addition,many researchers [19,40,41] have reported that using a turbulent model can better predict the micro-combustion behaviors above a certain Re. Their conclusions have been confirmed by experimental data. For example, Zhang et al. [40] reported that the turbulence model can get a much better prediction than the laminar model as compared with their experimental data. Ivan and Ahsan [41] showed that using a turbulent model

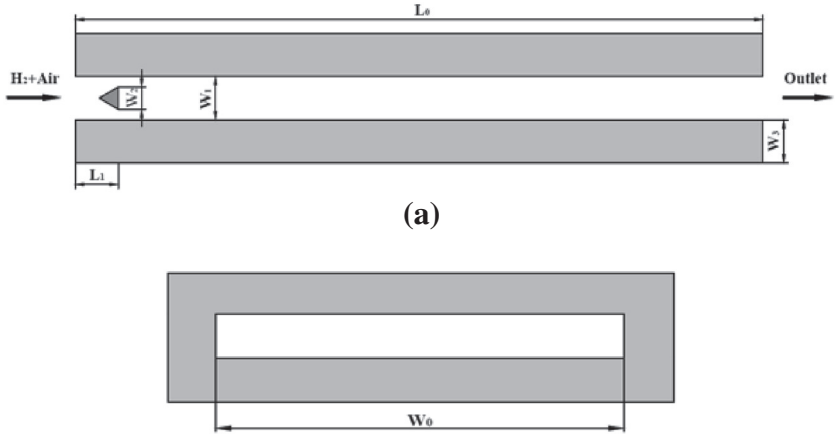

Fig. 1. Schematic diagram of the micro bluff body combustor [31]: (a) longitudinal cross section of the combustor, (b) combustor exit.

better predicted the diffusion combustion behaviors in a micro-combustor. Kuo and Ronney [19] also suggest that it is more appropriate to predict the combustion characteristics in micro-combustors by using a turbulence model when the Reynolds number is above ~500. It is worthy pointing out that they used the standard*k*-epsilon turbulent model in their work. In our case, the corresponding inlet velocity for *Re* = 500 is ~8.0 m/s. As to the micro bluff body combustor, our main concern is its blow-off limit which is much larger than 8.0 m/s (refer to Section 3.2). Besides, in our previous work [31], we compared several turbulent models and reaction models and found that the realizable *k*-epsilon turbulence model best predicted the blow-off limit as compared with our experimental data. The realizable *k*-epsilon turbulent model is a relatively recent development and differs from the standard *k*-epsilon model. It can be effectively applied to simulate various flows, such as the rotating uniform shear flow, free jet,free mixed flow, tubular flow, boundary-layer flow, and flow with separation. Therefore, we apply this model in the present paper. The governing equations for the gaseous mixture are shown below:

continuity:

$$\mathrm{div}(\rho \boldsymbol{u}) = 0 \tag{1}$$

momentum:

$$X \text{ direction}: \quad \mathrm{div}(\rho u \boldsymbol{u}) = -\frac{\partial p}{\partial x} + \mathrm{div}(\mu \,\mathrm{grad}\, u) \tag{2}$$

$$Y \text{ direction}: \quad \mathrm{div}(\rho v \boldsymbol{u}) = -\frac{\partial p}{\partial y} + \mathrm{div}(\mu \,\mathrm{grad}\, v) \tag{3}$$

energy:

$$\mathrm{div}(\rho \boldsymbol{u} h) = \mathrm{div}(k_f \,\mathrm{grad}\, T) + \sum_i \mathrm{div}(h_i \rho D_{i,m} \,\mathrm{grad}\, Y_i) + \sum_i h_i R_i \tag{4}$$

species:

$$\mathrm{div}(\rho \boldsymbol{u} Y_i) = \mathrm{div}(D_{i,m} \,\mathrm{grad}\,(\rho Y_i)) + R_i \tag{5}$$

where Y_i denotes the mass fraction of species i; R_i is the generation or consumption rate of species i; h_i is the enthalpy of species i, and k_f is the thermal conductivity of fluid; $\boldsymbol{u}$ is the velocity vector; u and v are the x and y direction components of the $\boldsymbol{u}$, respectively; μ is the dynamic viscosity of the fluid. $D_{i,m}$ is the mass diffusion coefficient: $D_{i,m} = \frac{1-X_i}{\sum_{j,j\neq i} X_j/D_{i,j}}$,where $D_{i,j}$ is the dual mass diffusion coefficient of species i in the species j; X_i and X_j are the mole percent of species i and j, respectively.

The transport equations of turbulence energy k and its dissipation rate ε are shown in Eqs. (6) and (7), respectively.

$$\frac{\partial(\rho k u_i)}{\partial x_i} = \frac{\partial}{\partial x_j}\left[\left(\mu + \frac{\mu_t}{\sigma_k}\right)\frac{\partial k}{\partial x_j}\right] + G_k - \rho\varepsilon \tag{6}$$

$$\frac{\partial(\rho \varepsilon u_i)}{\partial x_i} = \frac{\partial}{\partial x_j}\left[\left(\mu + \frac{\mu_t}{\sigma_\varepsilon}\right)\frac{\partial \varepsilon}{\partial x_j}\right] + \rho C_1 E \varepsilon - \rho C_2 \frac{\varepsilon^2}{k + \sqrt{\upsilon\varepsilon}} \tag{7}$$

where $C_1 = \max\left(0.43, \frac{\eta}{\eta+5}\right)$, C_2 = 1.9, σ_k = 1.0, σ_ε = 1.2.

As heat conduction in the solid walls can affect the combustion significantly [18], heat transfer in both of the combustor walls and bluff body is considered in the present computation. The energy equation for the solid phase is given as:

$$\mathrm{div}(k_s \,\mathrm{grad}\, T) = 0 \tag{8}$$

where k_s is the thermal conductivity of solid material.

2.3. Computation scheme

In the present study, three kinds of solid materials, i.e., quartz, stainless steel (316L) and SiC, are used and their effects on the blow-off limit are compared. Temperature dependences of their thermophysical properties were incorporated using polynomial functions based on handbook values [42]. The density of the gas mixture is calculated using the ideal gas assumption, while the specific heat, viscosity, and thermal conductivity were calculated from a mass fraction weighted average of species properties.

The detailed chemical reaction mechanism of H_2/O_2 mixture reported by Li et al. [43] was used, which includes 13 species and 19 reversible elementary reactions. The thermodynamic and transport properties of the gaseous species could be found in the CHEMKIN databases [44,45]. The finite-rate model was selected to solve the interaction between the turbulent flow and combustion. This model computes the chemical source terms using the Arrhenius expression.

Boundary conditions are set as follows: uniform concentration and velocity distributions of premixed H_2/air mixture were specified at the inlet of micro-combustor. The inlet temperature of mixture was set at 300 K. At the exit, an outflow boundary condition was specified. Surface to surface radiation between the inner surfaces of the combustor is considered using the discrete ordinates (DO) model [19]. At the outer surface of the solid walls, the heat losses including natural convection and thermal radiation are calculated by Eq. (9).

$$q = h(T_{W,O} - T_\infty) + \varepsilon\sigma(T_{W,O}^4 - T_\infty^4) \tag{9}$$

where h is the natural convection heat transfer coefficient. Based on the classic empirical correlation in [46], the value of h can be evaluated to be around 20 W/m^2 K when the out wall temperature is 1000 K. On the other hand, the heat loss via natural convection is much less than that via thermal radiation. We checked that the variation of h had a negligible effect on the blow-off limit. Therefore, we used an approximate mean value (h = 20 W/m^2 K) in the present study. This value is typical and was applied by other researchers [47].$T_{W,O}$ is the outer wall temperature and the ambient temperature T_∞ takes a constant value of 300 K. ε is the emissivity of the solid surface, and σ is the Stephan–Boltzmann constant with a value of 5.67×10^{-8} W/(m^2 K^4).

FLUENT 6.3 [48] was applied to solve the conservation equations of mass, momentum, energy and species as well as the conjugated heat conduction in solid materials. The second-order upwind scheme was used for discretization and the "SIMPLE" algorithm was employed for the pressure–velocity coupling. A non-uniform square grid system was employed and grid independence of the results was verified. The convergence of CFD simulation was judged upon residuals of all governing equations. Results reported here were achieved with residuals smaller than 1.0×10^{-6}.

3. Results and discussion

3.1. Model validation

In our previous study [31], the present numerical model has been validated by the experimental data, as shown in Fig. 2. It can be seen from Fig. 2 that the predicted blow-off limits agree reasonably well with the counterparts of the experiment. The relative errors between the numerical and experimental results are 5.3%, 12.2% and 5.8% for the equivalence ratios of 0.4, 0.5 and 0.6, respectively. This confirms the reasonable accuracy of the numerical model adopted in the present paper.

3.2. Effect of the solid material on the blow-off limit

Fig. 3 depicts the blow-off limits of the micro-combustors made of different solid materials, in which the numbers 1, 2 and 3 indicate quartz, stainless steel and SiC, respectively. The thermal

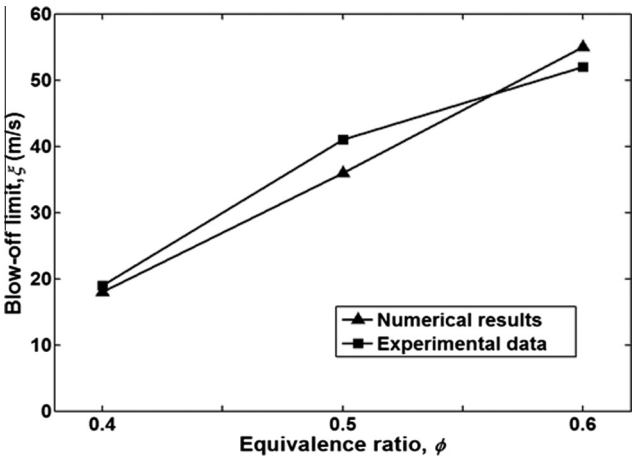

Fig. 2. Experimental and numerical results of blow-off limits for different equivalence ratios [31].

conductivities at 300 K are 1.18 W/(m K), 12.63 W/(m K), and 52.08 W/(m K) for quartz, stainless steel and SiC, respectively [42]. The blockage ratios of the three micro-combustors are the same of 0.5. It is seen from Fig. 3 that, when the equivalence ratio is the same, the blow-off limit of the quartz combustor is the largest, followed by that of the stainless steel combustor, and the SiC combustor has the smallest one. Khandelwal et al. [28] also found that stable combustion range of a combustor with backward steps can be extended when the solid walls are made of materials with lower thermal conductivity, which is consistent with the present study. However, our conclusion and that of Khandelwal et al. [28] are opposite to the results for the straight channel by Vlachos and co-workers [35–37]. The underlying mechanisms will be discussed in the following.

It is expected that flame stabilization in the micro bluff body combustor is affected by flow field and heat transfer processes as well as their interactions. For the convenience of discussion, we here define a 'recirculation zone' behind bluff body. The area where the longitudinal velocity component $V_x \leqslant 0$ is defined as the recirculation zone, and the longest distance from the contour of $V_x = 0$ to the right wall of bluff body is defined as the length of the recirculation zone. Similarly, a 'low velocity zone' is defined as the region of $0 < v_x \leqslant 20$ m/s to indicate the area with relatively lower velocity. The recirculation zone and low velocity zone play an important role in anchoring the flame root. In addition, the heat losses ratio, Φ, is defined in Eq. (10) to indicate the ratio of heat losses from the outer walls, Q', to the input enthalpy involved in the fuel, Q.

$$\Phi = Q'/Q \tag{10}$$

Detailed discussion will be given in the following texts.

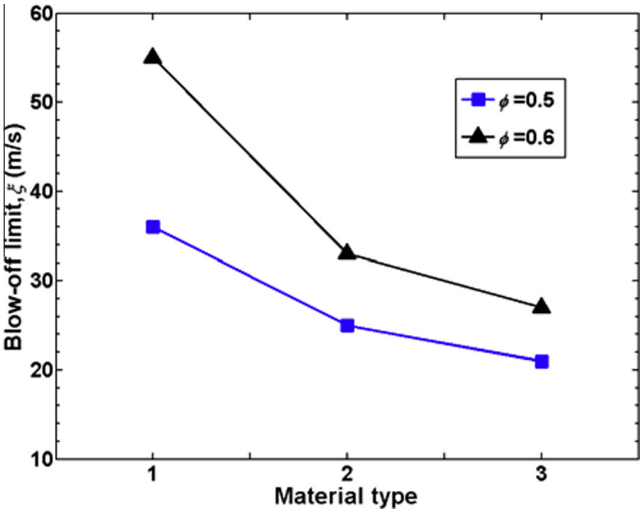

Fig. 3. Blow-off limits of the micro-combustors for different equivalence ratios: 1, 2 and 3 indicate quartz, stainless steel and SiC, respectively.

3.3. Discussion

Fig. 4 shows the contours of the longitudinal velocity component in the vicinity of the bluff body (axial distance $\leqslant$2.2 mm) in the combustors made of different solid materials. The inlet velocities are the same of 15 m/s. It is seen from Fig. 4 that the areas of recirculation zones are almost the same due to the identical blockage ratios of the three cases. However, it is clearly noticed that the low velocity zone for the quartz combustor is much larger than the other two cases. Fig. 5 illustrates the contours of the vertical velocity component near the bluff body (axial distance $\leqslant$2.2 mm) of the three micro-combustors. This figure shows that the velocity gradients, $\partial v/\partial x$, for the stainless steel combustor and SiC combustor are much larger than the quartz combustor, which leads to

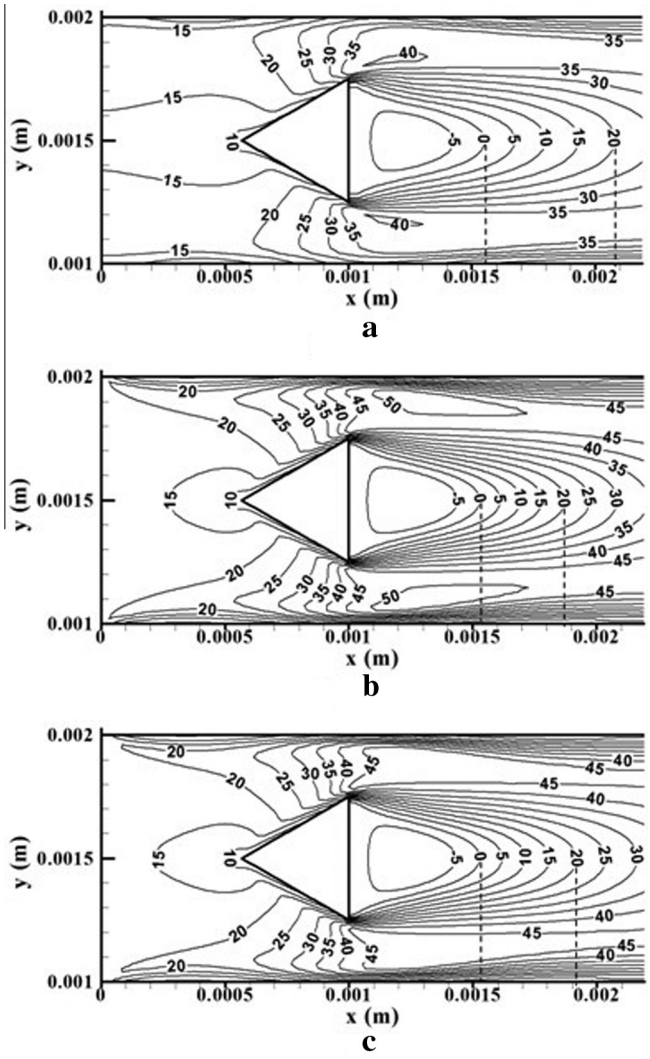

Fig. 4. Contours of the longitudinal velocity component near the bluff body ($0 < x < 2.2$ mm) at an inlet velocity of 15 m/s: (a) quartz, (b) stainless steel, (c) SiC. The equivalence ratios are the same of 0.5.

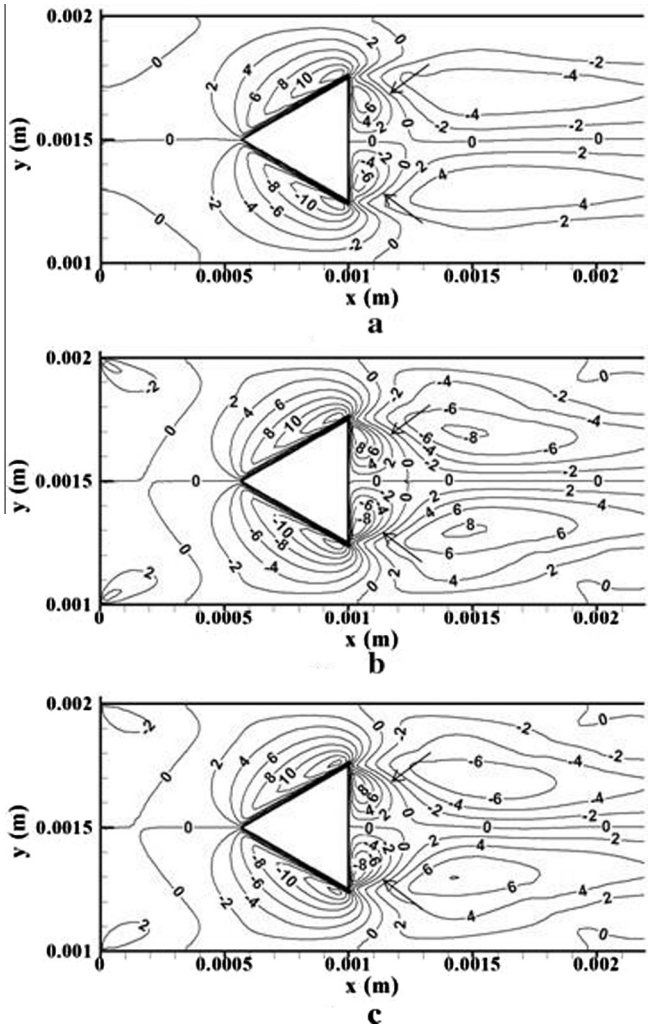

Fig. 5. Contours of the vertical velocity component near the bluff body ($0 < x < 2.2$ mm) at an inlet velocity of 15 m/s: (a) quartz, (b) stainless steel, (c) SiC. The equivalence ratios are the same of 0.5.

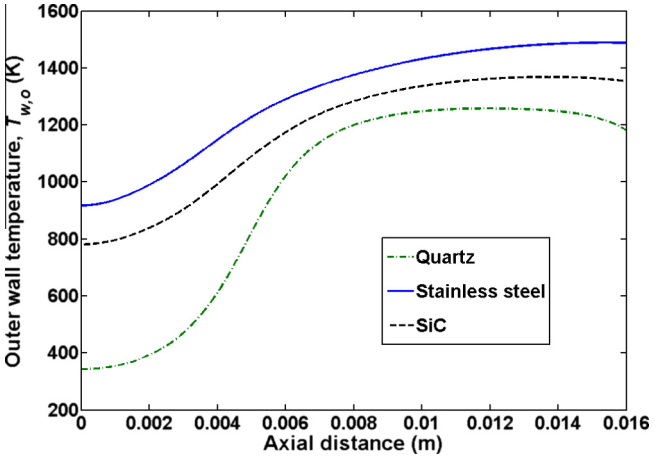

Fig. 6. Outer wall temperature profiles of the combustors made of different solid materials at the same inlet velocity of 15 m/s. The equivalence ratios are the same of 0.5.

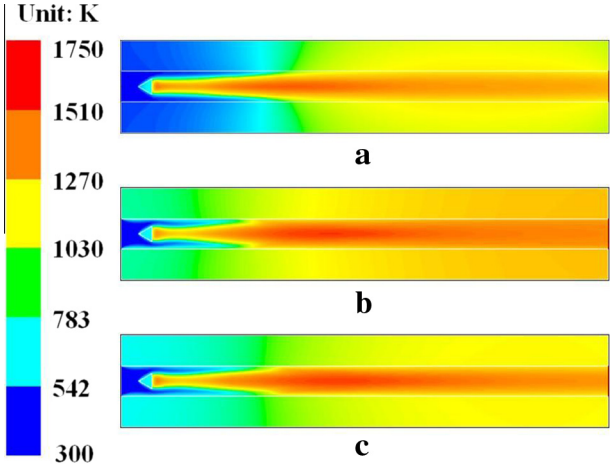

Fig. 7. Temperature fields of the combustors made of different solid materials: (a) quartz, (b) stainless steel, (c) SiC. The inlet velocities are the same of 15 m/s and the equivalence ratios are the same of 0.5.

stronger shear stresses for these two cases. Consequently, the flame stretching effect in the stainless steel combustor and SiC combustor are more pronounced which results in smaller blow-off limits for these two combustors as compared with the quartz combustor.

The reason for this phenomenon lies in the difference of solid materials. As have mentioned above, the thermal conductivities of stainless steel and SiC are much larger than that of quartz. Therefore, far more heat is transferred from downstream to upstream walls, which makes their wall temperature profiles much different from that of the quartz, as shown in Fig. 6. From Fig. 6, one can see that the wall temperature levels for stainless steel combustor and SiC combustor are much higher than that of quartz combustor. Moreover, wall temperature profiles are more uniform for the former two cases. The most important thing is that the wall temperatures on the two sides of the bluff body (1.0 mm < axial distance < 1.5 mm) are up to 500–600 K higher for the stainless steel combustor and SiC combustor. Therefore, the preheating effect of upstream wall on the fresh cold mixture is much better for the stainless steel combustor and SiC combustor, which can be clearly seen from the temperature fields, as shown in Fig. 7. From Fig. 7, it is evident that gas temperature near the inner walls of the upstream is much higher for the stainless steel combustor and SiC combustor, which leads to remarkable volumetric expansion and thus flow acceleration of the gas mixture in the upper and lower regions of the bluff body. Consequently, the low velocity zones of these two cases are much smaller and the shear stresses of these two combustors are much stronger as compared with the quartz combustor, as depicted in Figs. 4 and 5. The heat recirculation via the solid walls would also lead to an increase in the burning velocity [33,34]. However, this has two-sided effects. On the one hand, an increase in the burning velocity has a positive effect on the blow-off limit. On the other hand, an increase in the burning velocity would result in a more obvious volumetric expansion of the gaseous mixture, which has a negative effect on the blow-off limit.

The different characteristics of flow fields exert a significant action on the reaction zones which are usually indicated by the contours of a key radical OH. For comparison, reaction zones of the three cases at an inlet velocity of 15 m/s are presented in Fig. 8. From Fig. 8 it is obviously noted that in the stainless steel combustor and SiC combustor, reaction zones are more intensively stretched and start to split due to the stronger shear stress in the shear layers (interfaces between recirculation zone and low

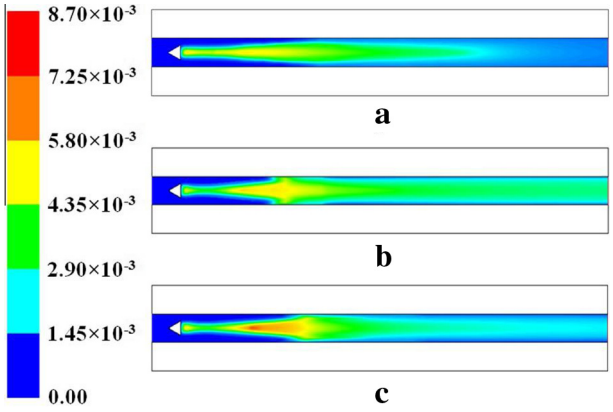

Fig. 8. Mass fraction contours of the radical OH in the combustors made of different solid materials: (a) quartz, (b) stainless steel, (c) SiC. The inlet velocities are the same of 15 m/s and the equivalence ratios are the same of 0.5.

velocity zone behind the bluff body). With further increase in the inlet velocity, the reaction zones will be more seriously prolonged and complete splitting of reaction zones will occur. We present the reaction zones near the blow-off limits of the three combustors in Fig. 9. This figure demonstrates that the reaction zone of the quartz combustor almost splits into two parts when the inlet velocity is increased to 36 m/s. For the stainless steel combustor and SiC combustor, the corresponding inlet velocity at which the reaction zones split are around 25 m/s and 21 m/s, respectively. With a slightly further increase in the inlet velocity, the two reaction zones will be totally separated and flame cannot sustain by solely depending on the smaller reaction zone in the recirculation zone. Consequently, flame blowout occurs. This phenomenon is verified by our previous experimental investigation of the quartz combustor, as shown in Fig. 10. This picture is directly taken with a digital camera under the blow-off limit condition. From this photograph it can also be seen that flame split into two parts before being blown out of the combustor.

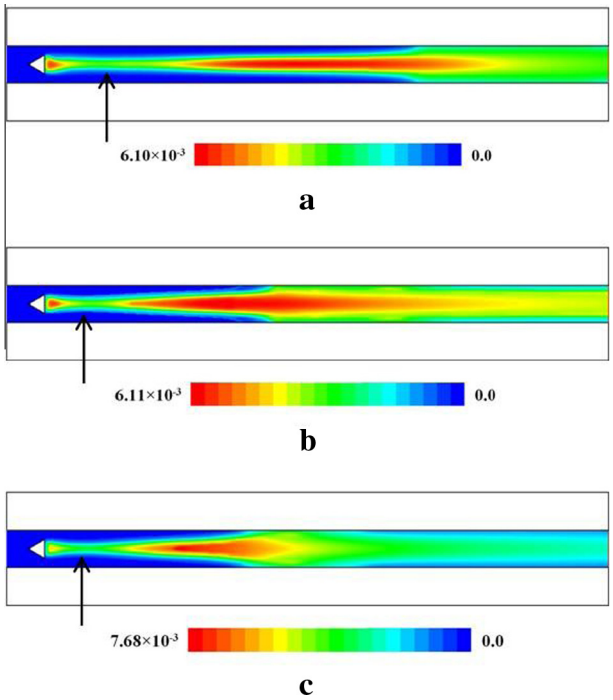

Fig. 9. Mass fraction contour of the radical OH near the blow-off limit in the combustors made of different solid materials: (a) quartz, the inlet velocity is 36 m/s, (b) stainless steel, the inlet velocity is 25 m/s, (c) SiC, the inlet velocity is 21 m/s. The equivalence ratios are the same of 0.5.

Fig. 10. Flame photograph directly taken with a digital camera in our previous experiment under the blow-off limit condition of the quartz combustor. The blockage ratio and equivalent ratio are both 0.5 [32].

Another thing should be elucidated is the difference between blow-off limits of the stainless steel combustor and SiC combustor. It can be noted from Fig. 4 that the low velocity zone of the SiC combustor is a little larger than that of the stainless steel combustor; however, the blow-off limit of the SiC combustor is less than that of the stainless steel combustor (see Fig. 3). This is caused by the difference in the heat losses ratios of these two micro-combustors. The heat losses ratios (including convection heat loss ratio Φ_{con}, radiation heat loss ratio Φ_{rad}, and the total heat losses ratio Φ_{tot}) of the three combustors are shown in Fig. 11. From this figure it is seen that the convection heat loss ratio of the stainless steel combustor is only 0.64% larger than that of SiC combustor; however, the radiation heat loss ratio of the SiC combustor is 15.11% larger than that of the stainless steel combustor. This is because the emissivity of the stainless steel is only ~0.20 while that of SiC is ~0.90. Thus, the total heat losses ratio of the SiC combustor is larger than the counterpart of the stainless steel combustor by 14.47%. Therefore, although the low velocity zone of the SiC combustor is a little larger than that of the stainless steel combustor (see Fig. 4), the blow-off limit of the SiC combustor is less than that of the stainless steel combustor due to its much larger total heat losses ratio which caused the wall temperature level of the SiC combustor to be lower than the stainless steel combustor (see Fig. 6). In addition, it is noteworthy from Fig. 11 that the total heat losses ratio of the quartz combustor (23.2%) is even higher than that of the stainless steel combustor (13.3%), although the wall temperature level of the quartz combustor is comparatively lower. This is because the emissivity of quartz (~0.92) is much larger than that of the stainless steel (~0.2).

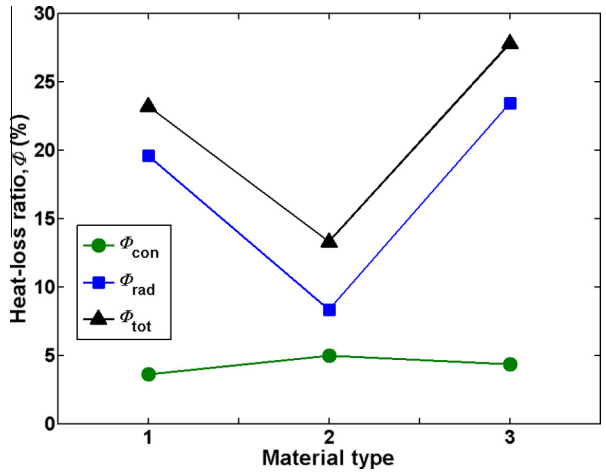

Fig. 11. Heat losses ratios of the combustors made of different solid materials: 1, 2 and 3 indicate quartz, stainless steel and SiC, respectively. Φ_{con}, Φ_{rad}, and Φ_{tot} denote convection heat loss ratio, radiation heat loss ratio, and the total heat losses ratio, respectively. The equivalence ratio is 0.5 and the inlet velocity is 10 m/s.

4. Conclusions

The effect of solid material on the blow-off limit of a micro bluff body combustor was numerically investigated. The results show that, at the identical blockage ratio and the same equivalence ratio, the blow-off limit of the quartz combustor is the largest, followed by that of the stainless steel combustor, and SiC combustor has the smallest one. The underlying mechanisms were discussed from the interactions among the flow field, heat transfer processes and flame stabilization. The analyses demonstrated that when the thermal conductivity is larger, more heat is transferred to the upstream walls and the fresh mixture is better preheated. Thus, the gaseous volume expands more dramatically, which leads to a smaller low velocity zone (although the recirculation zones for the three cases are almost the same). Therefore, the blow-off limit of the quartz combustor is larger than the stainless steel combustor and SiC combustor. Analyses of the reaction zones show that the flame blowout is caused by the stretching effect of the shear layers. When the inlet velocity is near the blow-off limit, the reaction zones are seriously prolonged and almost split into two parts. Further increase in the inlet velocity will lead to complete splitting of the reaction zone. As a result, flame blowout occurs because the flame cannot sustain solely depending on the small part of reaction zone behind the bluff body.

Although the low velocity zone of the SiC combustor is a little larger than that of the stainless steel combustor, it has a comparatively smaller blow-off limit. This difference mainly arises from their heat losses ratios. Because the emissivity of SiC ($\sim$0.90) is much larger than that of the stainless steel ($\sim$0.20), the total heat losses ratio of the SiC combustor is larger than the counterpart of the stainless steel combustor by 14.47%, which causes the SiC combustor to have a comparatively smaller blow-off limit.

In summary, solid materials with relatively low thermal conductivity and emissivity are beneficial to obtain a large blow-off limit for the micro bluff body combustor. This provides some guidance to develop micro-combustors with a wide operational range. The present study also shows that flow and heat transfer processes, as well as their strong interactions, have significant effect on flame stabilization in micro-combustors.

Acknowledgments

This work was supported by the Natural Science Foundation of China (Grant Nos. 51076054, 51276073, 51161140330, 51076053) and the Foundation of Key Laboratory of Low-grade Energy Utilization Technologies and Systems, Chongqing University, China.

References

[1] K. Maruta, Micro and mesoscale combustion, Proceedings of the Combustion Institute 33 (2011) 125–150.
[2] Y.G. Ju, K. Maruta, Microscale combustion: technology development and fundamental research, Progress in Energy and Combustion Science 37 (2011) 669–715.
[3] J.W. Li, B.J. Zhong, Experimental investigation on heat loss and combustion in methane/oxygen micro-tube combustor, Applied Thermal Engineering 28 (2008) 707–716.
[4] K. Maruta, T. Kataoka, N.I. Kim, S. Minaev, R. Fursenko, Characteristics of combustion in a narrow channel with a temperature gradient, Proceedings of the Combustion Institute 30 (2005) 2429–2436.
[5] F. Richecoeur, D.C. Kyritsis, Experimental study of flame stabilization in low Reynolds and Dean number flows in curved mesoscale ducts, Proceedings of the Combustion Institute 30 (2005) 2419–2427.
[6] A.W. Fan, S. Minaev, E. Sereshchenko, Y. Tsuboi, H. Oshibe, H. Nakamura, K. Maruta, Propagation dynamics of splitting flames in a heated microchannel, Combustion, Explosion and Shock Waves 45 (2009) 245–250.
[7] S. Minaev, K. Maruta, R. Fursenko, Nonlinear dynamics of flame in a narrow channel with a temperature gradient, Combustion Theory and Modeling 11 (2007) 187–203.
[8] T.L. Jackson, J. Buckmaster, Z. Lu, D.C. Kyritsis, L. Massa, Flames in narrow circular tubes, Proceedings of the Combustion Institute 31 (2007) 955–962.
[9] G. Pizza, C.E. Frouzakis, J. Mantzaras, A.G. Tomboulides, K. Boulouchos, Dynamics of premixed hydrogen/air flames in microchannels, Combustion and Flame 152 (2008) 433–450.
[10] S. Minaev, E. Sereshchenko, R. Fursenko, A.W. Fan, K. Maruta, Splitting flames in a narrow channel with a temperature gradient in the walls, Combustion, Explosion and Shock Waves 45 (2009) 119–125.
[11] H. Nakamura, A.W. Fan, S. Minaev, E. Sereshchenko, R. Fursenko, Y. Tsuboi, K. Maruta, Bifurcations and negative propagation speeds of methane/air premixed flames with repetitive extinction and ignition in a heated microchannel, Combustion and Flame 159 (2012) 1631–1643.
[12] S. Kumar, K. Maruta, S. Minaev, Pattern formation of flames in radial microchannels with lean methane–air mixtures, Physical Review E 75 (2007) 016208.
[13] A.W. Fan, S. Minaev, S. Kumar, W. Liu, K. Maruta, Regime diagrams and characteristics of flame patterns in radial microchannels, Combustion and Flame 153 (2008) 479–489.
[14] A.W. Fan, K. Maruta, H. Nakamura, S. Kumar, W. Liu, Experimental investigation on flame pattern formations of DME–air mixtures in a radial microchannel, Combustion and Flame 157 (2010) 1637–1642.
[15] A.W. Fan, J.L. Wan, K. Maruta, H. Nakamura, H. Yao, W. Liu, Flame dynamics in a heated meso-scale radial channel, Proceedings of the Combustion Institute 34 (2013) 3351–3359.
[16] A.A. Deshpande, S. Kumar, On the formation of spinning flames and combustion completeness for premixed fuel/air mixtures in stepped tube microcombustors, Applied Thermal Engineering 51 (2013) 91–101.
[17] M. Akram, S. Kumar, Experimental studies on dynamics of methane–air premixed flame in meso-scale diverging channels, Combustion and Flame 158 (2011) 915–924.
[18] N.I. Kim, S. Kato, T. Kataoka, T. Yokomori, S. Maruyama, T. Fujimori, K. Maruta, Flame stabilization and emission of small Swiss-roll combustors as heaters, Combustion and Flame 141 (2005) 229–240.
[19] C.H. Kuo, P.D. Ronney, Numerical modeling of non-adiabatic heat-recirculating combustors, Proceedings of the Combustion Institute 31 (2007) 3277–3284.
[20] B.J. Zhong, J.H. Wang, Experimental study on premixed CH_4/air mixture combustion in micro Swiss-roll combustors, Combustion and Flame 157 (2010) 2222–2229.
[21] J. Li, S.K. Chou, Z.W. Li, W.M. Yang, Experimental investigation of porous media combustion in a planar micro-combustor, Fuel 89 (2010) 708–715.
[22] J.R. Shi, M.Z. Xie, G. Li, H. Liu, J.T. Liu, H.T. Li, Approximate solutions of lean premixed combustion in porous media with reciprocating flow, International Journal of Heat and Mass Transfer 52 (2009) 702–708.
[23] J.R. Shi, M.Z. Xie, Z.J. Xue, Y.N. Xu, H.S. Liu, Experimental and numerical studies on inclined flame evolution in packing bed, International Journal of Heat and Mass Transfer 55 (2012) 7063–7071.
[24] L.Q. Jiang, D.Q. Zhao, X.H. Wang, W.B. Yang, Development of a self-thermal insulation miniature combustor, Energy Conversion and Management 50 (2009) 1308–1313.
[25] U.W. Taywade, A.A. Deshpande, S. Kumar, Thermal performance of a micro combustor with heat recirculation, Fuel Processing Technology 109 (2013) 179–188.
[26] W.M. Yang, S.K. Chou, C. Shu, Z.W. Li, H. Xue, Combustion in micro-cylindrical combustors with and without a backward facing step, Applied Thermal Engineering 22 (2002) 1777–1787.
[27] J.F. Pan, J. Huang, D.T. Li, W.M. Yang, W.X. Tang, H. Xue, Effects of major parameters on micro-combustion for thermophotovoltaic energy conversion, Applied Thermal Engineering 27 (2007) 1089–1095.
[28] B. Khandelwal, G.P.S. Sahota, S. Kumar, Investigations into the flame stability limits in a backward step micro scale combustor with premixed methane–air mixtures, Journal of Micromechanics and Microengineering 20 (2010) 095030.
[29] M. Wu, J. Hua, K. Kumar, An improved micro-combustor design for micro gas turbine engine and numerical analysis, Journal of Micromechanics and Microengineering 15 (2005) 1817–1823.
[30] A. Mehra, X. Zhang, A.A. Ayon, I.A. Waitz, M.A. Schmidt, C.M. Spadaccini, A six-wafer combustion system for a silicon micro gas turbine engine, Journal of Microelectromechanical System 9 (2000) 517–527.
[31] J.L. Wan, A.W. Fan, K. Maruta, H. Yao, W. Liu, Experimental and numerical investigation on combustion characteristics of premixed hydrogen/air flame in a micro-combustor with a bluff body, International Journal of Hydrogen Energy 37 (2012) 19190–19197.
[32] A.W. Fan, J.L. Wan, Yi Liu, B.M. Pi, H. Yao, K. Maruta, W. Liu, The effect of the blockage ratio on the blow-off limit of a hydrogen/air flame in a planar micro-combustor with a bluff body, International Journal of Hydrogen Energy (2013), http://dx.doi.org/10.1016/j.ijhydene.2013.06.100
[33] A. Veeraragavan, C. Cadou, Experimental investigation of influence of heat recirculation on temperature distribution and burning velocity in a simulated micro-burner, in: 45th AIAA Aerospace Sciences Meeting and Exhibit, 8–11 January, 2007, Reno, Nevada.
[34] A. Veeraragavan, C. Cadou, Flame speed predictions in planar micro/mesoscale combustors with conjugate heat transfer, Combustion and Flame 158 (2011) 2178–2187.
[35] D.G. Norton, D.G. Vlachos, A CFD study of propane/air microflame stability, Combustion and Flame 138 (2004) 97–107.

[36] N.S. Kaisare, D.G. Vlachos, Optimal reactor dimensions for homogeneous combustion in small channels, Catalysis Today 120 (2007) 96–106.
[37] J.A. Federici, D.G. Vlachos, A computational fluid dynamics study of propane/air microflame stability in a heat recirculation reactor, Combustion and Flame 153 (2008) 258–269.
[38] A. Beskok, G.E. Karniadakis, A model for flows in channels pipes, and ducts at micro and nano scales, Microscale Thermophysical Engineering 3 (1999) 43–77.
[39] F.A. Williams, Combustion Theory the Fundamental Theory of Chemically Reacting Systems, second ed., Benjamin/Cummings Publ. Co., Menlo Park, CA, 1985.
[40] Y.S. Zhang, J.H. Zhou, W.J. Yang, M.S. Liu, K.F. Cen, Study on the model selection for micro-combustion simulation, Proceedings of the Chinese Society for Electrical Engineering 26 (2006) 81–87 (in Chinese).
[41] A.A. Ivan, R.C. Ahsan, Numerical investigation on the mixing behavior of micro combustors, in: Proceedings of ASME 2003 Design Engineering Technical Conferences and Computers and Information in Engineering Conference, Chicago, Illinois, USA, 2003.
[42] Q.F. Ma, R.S. Fang, L.C. Xiang, Handbook of Thermo-Physical Properties, China Agricultural Machinery Press, Beijing, 1986 (in Chinese).
[43] J. Li, Z.W. Zhao, A. Kazakov, F.L. Dryer, An updated comprehensive kinetic model of hydrogen combustion, International Journal of Chemical Kinetics 36 (2004) 1–10.
[44] R.J. Kee, F.M. Rupley, J.A. Miller, The CHEMKIN thermodynamic database, Sandia National Laboratories, Report SAND87-8215B; 1990.
[45] R.J. Kee, J.F. Grear, M.D. Smooke, J.A. Miller, A Fortran program for modeling steady laminar one-dimensional premixed flames, Sandia National Laboratories Report SAND 85-8240, 1985.
[46] J.P. Holman, Heat Transfer, ninth ed., McGraw-Hill, New York, 2002.
[47] G.B. Chen, Y.C. Chao, C.P. Chen, Enhancement of hydrogen reaction in a micro-channel by catalyst segmentation, International Journal of Hydrogen Energy 33 (2008) 2586–2595.
[48] Fluent 6.3 User's Guide, Lebanon, Fluent Inc., New Hampshire, 2006.